PREVENTION OF FORWARD SWEPT WING AEROELASTIC INSTABILITIES WITH ACTIVE CONTROLS

T. E. Noll
Aerospace Engineer
U.S. Air Force Wright Aeronautical Laboratories
Flight Dynamics Lab
WPAFB OH

F. E. Eastep
Professor and Director
Graduate Aerospace Engineering Dept
University of Dayton, OH

and

R. A. Calico
Professor
U.S. Air Force Institute of Technology
WPAFB OH

Abstract

Analyses were conducted to investigate the feasibility of using feedback control systems for preventing multiple aeroelastic instabilities in close proximity on forward swept wing aircraft with or without external stores. With the addition of wing mounted external stores, the bending/torsion flutter speed can be driven lower into the vicinity of the aeroelastic instability speeds more commonly associated with a forward swept wing (divergence or body freedom flutter). This paper presents the results of analyses using a typical flexible forward swept wing undergoing various rigid body motions. Pade polynomial approximations of the unsteady aerodynamic force coefficients and a root locus procedure are applied in obtaining a suitable design. The analyses indicated that an active system using a leading edge control surface commanded by displacement feedback (for suppressing the divergence tendencies of the first bending mode) and a trailing edge surface using angular acceleration feedback (for preventing the bending/torsion flutter mode) resulted in significant increases in the flight envelope for the configurations studied. Also, the adequacy and sensitivity of the active system over the velocity range of interest was explored and an evaluation of the effects of other critical feedback parameters of interest was conducted. This paper demonstrated the usefulness of such a concept for application to forward swept wing technology and established a requirement for more detailed analyses and wind tunnel tests to increase the level of confidence needed in the future for concept acceptance as a design option.

I. Introduction

The forward swept wing has been long recognized as able to provide some improved aerodynamic performance benefits over the aft swept wing design, provided the weight needed to solve the potential aeroelastic problems (divergence) can be made small. One design technique for preventing static divergence was suggested by Krone [1] and involved the tailoring of laminated composite materials. Since composite fiber materials have higher specific stiffness and strength characteristics than conventional metals and have directional properties, the orientation of the fibers in a particular direction can change the deformation of the wing under aerodynamic loading. Therefore, the tailoring of advanced composite materials can reduce the wash-in of the forward swept wing and increase the divergence speed.

Another procedure which has been shown to offer significant promise for preventing aeroelastic instabilities involves the use of active controls technology. The principles and procedures of applying these concepts are well documented as a result of the significant amount of research performed in the 1970's to develop active flutter suppression technology and in the early 1980's to advance digital flight control and adaptive control principles. Griffin and Eastep[2] have performed calculations to apply these principles to delay the onset of divergence of forward swept wings and have obtained results which were as successful as the results from previous flutter suppression applications.

Recent studies that involved analyses[3] and tests[4] on a forward swept wing encountered low speed dynamic instabilities when the rigid body pitch degree of freedom was allowed. This instability has been described as pitch/bending flutter or body freedom flutter. This low velocity instability involves coupling of the aircraft short period mode and a wing bending mode. To further describe the phenomenon, Figure 1 illustrates the behavior of the critical modes for both a forward and aft swept wing. For a cantilever forward swept wing, the bending mode frequency drops with increasing speed until it becomes zero and static divergence occurs. For a forward swept wing aircraft free in pitch, the bending mode frequency still drops but the presence of the short period mode at a lower frequency causes a coalescence of the two modes resulting in a low speed dynamic instability. This instability has been found[5,6] in rare instances in the past on straight or slightly aft swept wing aircraft. For an aft swept wing aircraft classical coupling of the wing torsion

mode with a wing bending mode results in bending/torsion flutter whether the model is cantilevered or free in pitch. Although body freedom flutter is calculated to be more critical than divergence of a cantilever forward swept wing, one should not generalize these findings. It is conceivable that wing divergence may, for peculiar forward swept wing aircraft configurations, be the most critical aeroelastic instability. Therefore, divergence of a cantilever wing should not be disregarded in the development of any new and promising aeroelastic control procedures.

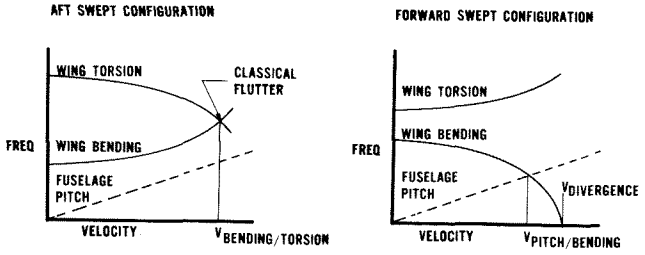

Figure 1 Flutter with Fuselage Pitch Degree of Freedom

Active control system analyses have also been conducted for the forward swept wing with rigid pitch motion included.[7-10] Results from these analyses were also very favorable in terms of suppressing the body freedom flutter instability to a desired airspeed.

Future weapon requirements which are hampered by inflationary costs define the need for a multimission fighter. It is speculated that a forward swept wing fighter would evolve in operational deployment similar to what had occurred in the past for aft swept wing fighters. The forward swept wing fighter would probably be designed for a primary mission but would be used in off-design missions for air-to-ground sorties. To obtain this multirole capability, the forward swept wing fighter would need to carry external stores conformally on the fuselage and under the wings. However, the adverse mass and inertia distribution on the wings caused by the external stores have traditionally resulted in severe bending/torsion flutter problems restricting aircraft to lower speeds and smaller payloads. External stores carried by a forward swept wing fighter would cause the higher frequency bending/torsion flutter mode to drop within the flight envelope of the vehicle or come in close proximity to the aeroelastic instabilities more commonly associated with the forward swept wing. Conventional flutter prevention techniques of ballasting the wing, or stiffening the wing are not suited for solving store flutter problems. Also, the use of speed placards to avoid aeroelastic instabilities are not attractive since they can cause severe speed restrictions resulting in a degradation of aircraft performance and survivability.

The purpose of the present research is to demonstrate by analysis the potential for and feasibility of applying active feedback control systems for preventing, simultaneously: (1) divergence and a high frequency bending/torsion flutter mode (in close proximity) of a cantilever forward swept wing; and (2) the rigid body pitch/wing bending instability and flutter (in close proximity) associated with the wing free in pitch or free in pitch and plunge. The goal is to increase the onset of the lowest instability speed 20 percent above the wing bending/torsion flutter speed of each wing configuration.

II. Theoretical Development

The aeroelastic equations of motion of a flexible aircraft in the airstream are represented as

$$[M]\{\ddot{q}\} + [C]\{\dot{q}\} + [K]\{q\} = \{F\} \tag{1}$$

where $[M]$, $[C]$ and $[K]$ are the generalized mass, damping, and stiffness matrices obtained using a set of generalized coordinates $\{q\}$ and several natural vibration mode shapes, and $\{F\}$ represents the unsteady aerodynamic forces. The forces are obtained from the subsonic doublet lattice unsteady aerodynamic theory[11]. These forces are defined to be

$$\{F\} = -\frac{1}{2}\rho V^2 \bar{s}\,[Q(k)]\{q\} \tag{2}$$

where an element of the generalized aerodynamic force coefficient matrix $[Q]$ is computed from

$$Q_{ij} = \int\int \frac{\Delta p_j}{1/2\rho V^2}\,\frac{h_i}{\bar{s}}\,dx\,dy. \tag{3}$$

The coefficient Q_{ij} represents the force in the i^{th} mode due to pressure from the j^{th} mode and is dependent on the reduced frequency defined as

$$k = \frac{b\omega}{V}. \tag{4}$$

To obtain the unsteady aerodynamic forces in a polynomial representation of the Laplace variable for use with the root locus techniques, a Pade approximant[12] of the aerodynamics was considered. A Pade approximant was proposed by Vepa[13] as an aerodynamic force coefficient fitting function. To obtain the Pade approximants, a least squares fitting scheme was employed. The objective was to obtain the aerodynamic force coefficients in the form of

$$Q_{ij}(\bar{s}) = \left(\frac{N_0 + N_1\bar{s} + N_2\bar{s}^2 + N_3\bar{s}^3}{1 + D_1\bar{s} + D_2\bar{s}^2}\right)_{ij} \tag{5}$$

where $\bar{s} = \frac{bs}{V}$. (6)

A polynomial of this order was found to provide a good approximation to the generalized forces for the low subsonic speed range investigated.

The curve fitting was completed along the imaginary axis with respect to k, since here $\bar{s} = ki$. The coefficients N_i and D_i were obtained in two separate steps. Unique numerator and denominator polynomials were obtained using a least square fitting process for each of the aerodynamic force coefficient elements over the

reduced frequency range of interest. To reduce the number of roots associated with the aerodynamic fitting procedure, all the denominator polynomials were averaged together to obtain one common denominator. During the second step, the least square process was repeated with the denominator polynomials constrained to the averaged value obtained during the previous step.

The aeroelastic equations of motion of a flexible aircraft with control surfaces are described as

$$[M]\{\ddot{q}\} + [C]\{\dot{q}\} + [K]\{q\} + 1/2\rho V^2 \tilde{S}[Q]\{q\} + [M_c]\{\ddot{q}_c\} + 1/2\rho V^2 \tilde{S}[Q_c]\{q_c\} = 0, \quad (7)$$

where

$$\{q_c\} = \begin{Bmatrix} \delta_1 \\ \delta_2 \\ \cdot \\ \cdot \\ \cdot \\ \delta_i \end{Bmatrix} . \quad (8)$$

The control displacements, δ_i, are defined as

$$\delta_i = T_i(s) \lfloor h_i \rfloor \{q\} . \quad (9)$$

$T_i(s)$ represents the transfer functions in the Laplace variable in each of the feedback loops (gain, sensor dynamics, actuator dynamics, and the compensation), and $\lfloor h_i \rfloor$ defines the modal participation coefficients which relate the degree each of the rigid body or elastic modes participate in the wing motion at a particular location on the structure. For these analyses, sensor and actuator dynamics were neglected. With the feedback compensation and sensor types known, Equation (7) could be rearranged to appear as

$$[F_n]s^n + [F_{n-1}]s^{n-1} + \ldots + [F_1]s + [F_0] = 0 . \quad (10)$$

Equation (10) is a polynomial equation with constant matrix coefficients. These coefficients consist of not only the structural, aerodynamic and planform properties of the aircraft, but also velocity and the control system compensation (gain and phase). For these studies, the velocity and gain was varied independently to determine velocity and gain root locus plots. With all gains set to zero, Equation (10) reduces to a fourth order polynomial. An analysis for these conditions results in the passive (unaugmented) solution of the equations of motion. To obtain the roots of Equation (10), the procedure is to transform the equation into an eigenvalue problem of the form

$$([A] - s[I])\{q\} = 0. \quad (11)$$

III. Configuration Definition

Figure 2 presents a schematic of the model configuration selected for this study. The planform and stiffness characteristics of the model are those of a wind tunnel model previously tested[4] to investigate divergence and body freedom flutter trends. For this study, the mass and inertia of several wing sections was increased to simulate the effects of external stores. The selected model had a reference axis sweep angle of 15°, which corresponds to a wing leading edge sweep angle of 9°.

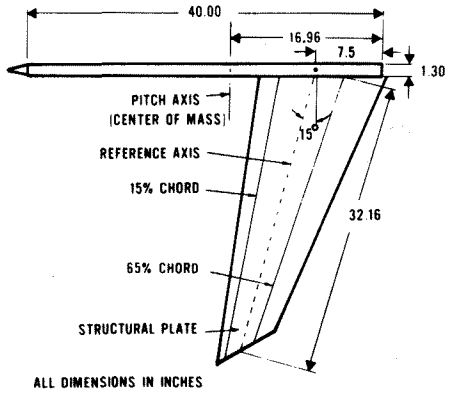

Figure 2 Planform of Forward Swept Wing Model

A finite element[14] representation of the configuration was developed to obtain the model vibration characteristics. The calculated node lines and associated frequencies for the first three modes of the model cantilevered, free in only rigid pitch, and free in both rigid pitch and plunge are shown in Figures 3 through 5 respectively.

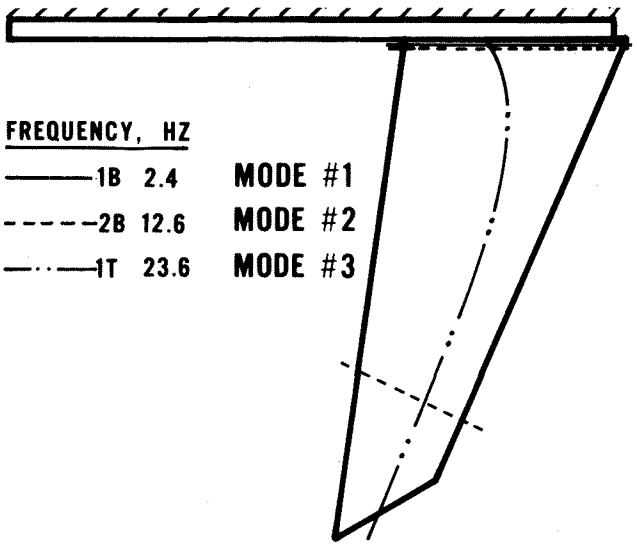

Figure 3 Calculated Frequencies and Node Lines of Cantilever Model

The aerodynamic paneling arrangement developed for the divergence and flutter analysis is shown in Figure 6. The paneling consisted of a fuselage with five interference panels and a slender body (not shown), and a wing with six aerodynamic panels subdivided into 104 boxes. Two of the outboard panels represent the leading edge and trailing edge control surfaces that were used in the control system analyses. These surfaces are positioned near the wing 3/4 span and have hinge lines parallel to the respective wing edges. Reduced frequency dependant unsteady aerodynamics for the model were calculated using

the doublet lattice method [11] and were then approximated by Pade polynomials as described in the previous section. Only the first three elastic modes were used in the aeroelastic and control design analyses, since higher frequency modes did not affect the passive flutter and divergence predictions, and were also outside the bandwidth of practical control systems.

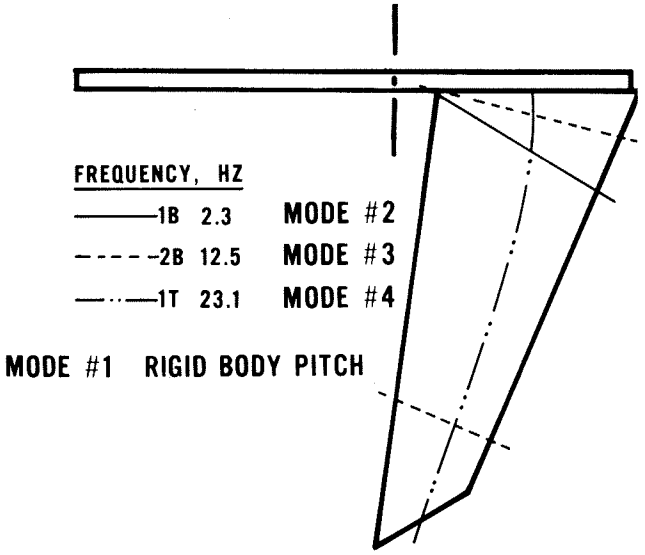

Figure 4 Calculated Frequencies and Node Lines of Model Free in Pitch

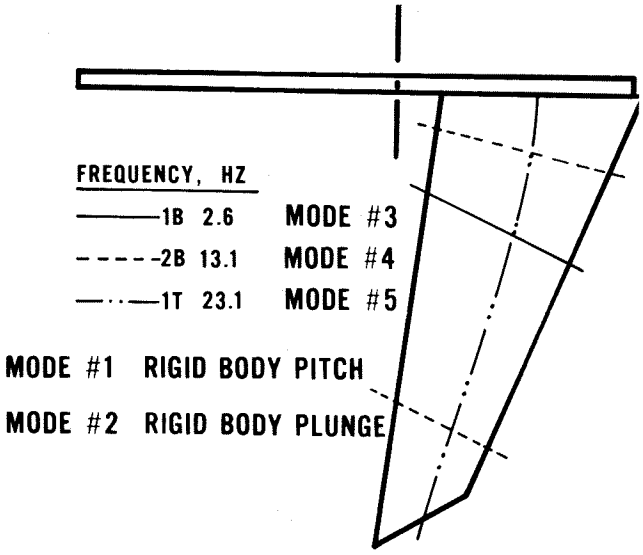

Figure 5 Calculated Frequencies and Node Lines of Model Free in Pitch and Plunge

Figure 7 presents a velocity root locus plot for the cantilever wing with all feedback gains set to zero (passive solution). The passive divergence speed (V_{DP}) was predicted to occur at 115 ft/sec and the passive bending/torsion flutter speed (V_{fp}) was predicted to occur at 156 ft/sec at a passive flutter frequency (ω_{fp}) of 16.7 Hz.

The velocity root locus plot for the model free in pitch with all systems off (passive solution) is presented in Figure 8. The body freedom flutter instability was predicted to

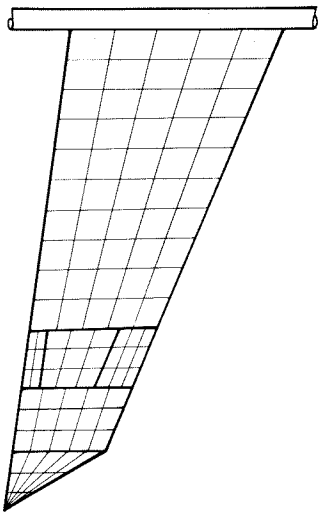

Figure 6 Aerodynamic Panel Representation of Wing with Leading and Trailing Edge Control Surfaces

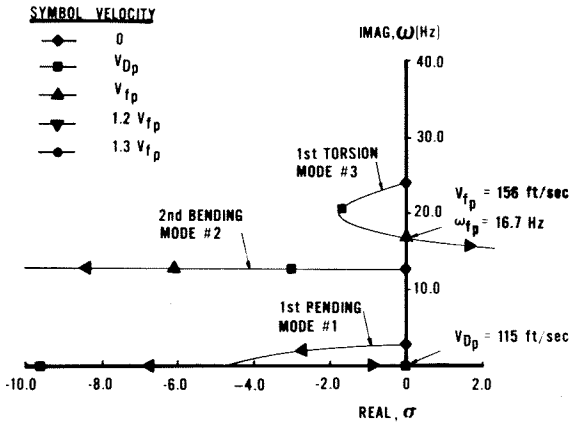

Figure 7 Root Locus Plot for the Cantilever Wing, Passive Solution

occur in the rigid pitch mode at 52 ft/sec at 1.2 Hz. This analysis predicted the higher frequency bending/torsion instability to occur at 151 ft/sec at 16.5 Hz. The passive flutter characteristics of the model free in both pitch and plunge are provided in Figure 9. For this configuration, coupling to produce the body freedom flutter mode caused the 1st bending mode to become unstable instead of the rigid pitch mode as was the case when the model was free in pitch only. The body freedom instability speed also increased somewhat with the addition of the rigid plunge mode. This increase in instability speed is at least partially attributed to the effect caused by a free-free boundary condition on the elastic modes. Body freedom flutter was predicted to occur at 72 ft/sec at 1.9 Hz. For the higher bending/torsion flutter instability, the analysis predicted a flutter speed of 152 ft/sec at 16.4 Hz.

IV. Design Approach

The approach used in determining the feedback compensation of the system for each model configuration was to obtain and evaluate gain loci plots associated with several sensor types and locations for different control surface

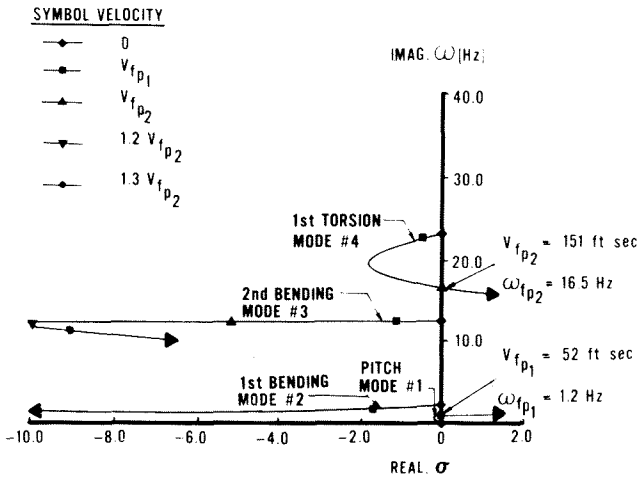

Figure 8 Root Locus Plot for the Model Free in Pitch, Passive Solution

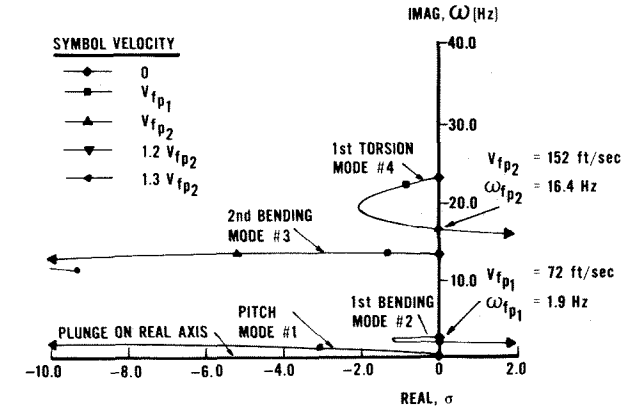

Figure 9 Root Locus Plot for the Model Free in Pitch and Plunge, Passive Solution

inputs at an airspeed 20 percent above the bending/torsion flutter speed. This information was used to determine the sensor/control surface combinations that provided the best capability for preventing the aeroelastic instabilities. Each control system design was then evaluated at off-design conditions to assure stability for the entire velocity range of interest and for appropriate changes in gains and phase angles.

A large number of sensor/control surface combinations were evaluated during the design of each control system. Only a few of the important combinations are presented for each wing configuration to illustrate the design process.

The next three figures present plots of the gain loci associated with the important sensor/control surface combinations of the cantilever wing at the design airspeed. Figure 10 provides a root locus for the transfer function that relates displacement to leading edge excitation (h/δ_{LE}). On this plot, the poles of the system represent the location of the roots of the elastic modes with the gains set to zero at the design velocity. At this speed, two of the poles are unstable. The first bending mode appears as two roots on the real axis, one of which is in the right half plane (static divergence). The other unstable mode is the 1st torsion mode which is shown as one of the roots of a complex pair at about 13.9 Hz. The 2nd bending mode located at about 11.9 Hz is stable at this airspeed. The solid circles on the chart represent the zeros of the control law (location of the root at infinite gain). The solid lines represent the path taken by the roots when the gain was increased from zero to positive infinity. Dash lines represent the path taken by the roots when the gain was decreased from zero to negative infinity. Figure 10 shows that negative gain brings the unstable real root back to the left side quite rapidly but high negative gains are required to stabilize the 1st torsion mode. It was found, however, that high negative gains destabilized other modes at off-design conditions leading to the conclusion that this signal/control surface combination could not be used alone to control both modes of instability simultaneously. For this control surface/sensor combination, a negative gain was selected such that the 1st bending mode was stable at the design airspeed with acceptable gain margins at V_{fp}. The gain was found to be -5.2 deg/in. This gain value is marked as the design gain on the loci of Figure 10.

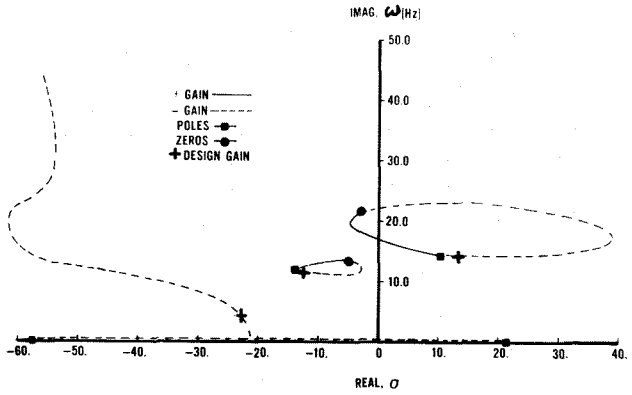

Figure 10 h Versus δ_{LE} Gain, Cantilever Wing, $V = 1.2\ V_{f_p}$

With the leading edge loop closed, the second loop using the trailing edge control surface and angular acceleration feedback was designed to stabilize the torsion mode at 1.2 V_{fp} with gain margins of at least $\pm$ 6db at V_{fp}. The gain loci for this combination of parameters is provided in Figure 11. This plot shows that two of the poles of the system, the 1st bending and 2nd bending, are stable at 1.2 V_{fp} as expected since the leading edge loop was closed. The torsion mode, however, still remains unstable for zero gain on the trailing edge system. Only negative feedback in a small range was successful in stabilizing the torsion mode. A trailing edge gain of -.025 deg/deg/sec^2 was required to stabilize the torsion mode at 1.2 V_{fp} and to provide the desired gain margins at V_{fp}.

To obtain maximum phase margins, a phase lag network of the form $\frac{1 - \tau s}{1 + \tau s}$ was included in the feedback compensation of the trailing edge system. This type of network has been used extensively in operational analog simulations to verify control system phase margins. It is ideal

for this use because large phase angles are possible with no gain changes. It was determined that the best phase characteristics for the cantilever wing were obtained when τ was .04223. This system provided 155 degrees of phase lag at a reference frequency of 17 Hz.

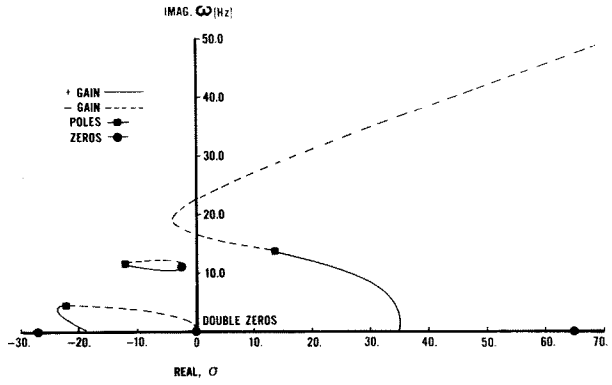

Figure 11 $\ddot{\alpha}$ Versus δ_{TE} Gain with K_{LE} = -5.20, Cantilever Wing, V = 1.2 V_{f_p}

Figure 12 shows the gain loci with the leading edge loop closed and the phase lag network included in the trailing edge loop compensation. The addition of the phase lag network results in a potentially unstable zero. However, the gain needed to drive the system unstable was found to be extremely high. The trailing edge design gain (.025 deg/deg/sec^2) is marked on the loci of Figure 12 for reference.

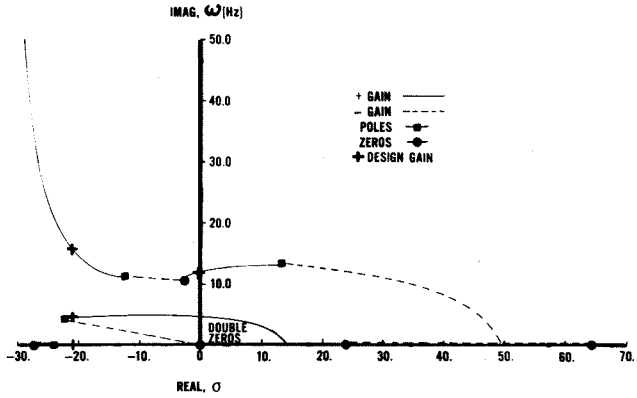

Figure 12 $\ddot{\alpha}$ Versus δ_{TE} Gain with K_{LE} = -5.20 and $\phi_{TE} = \frac{1 - .04223S}{1 + .04223S}$, Cantilever Wing, V = 1.2 V_{f_p}

Figures 13 through 15 present the gain root loci important in the design of the system for the model free in rigid pitch. The poles shown in Figure 13 represent the rigid pitch mode and the three elastic modes for the unaugmented model at 1.2 V_{fp2}. The poles on the negative real axis represent the 1st bending mode. The two unstable modes represent the rigid pitch mode at 2.5 Hz and the 1st torsion mode at 13.7 Hz. The stable 2nd bending mode is located at 11.9 Hz. Calculations using displacement feedback with the leading edge control surface indicate the possiblity of preventing both instabilities simultaneously with high negative gains. However, analyses at off-design conditions, that is at velocities lower than 1.2 V_{fp2}, predicted instabilities in other elastic modes as a result of the high gains.

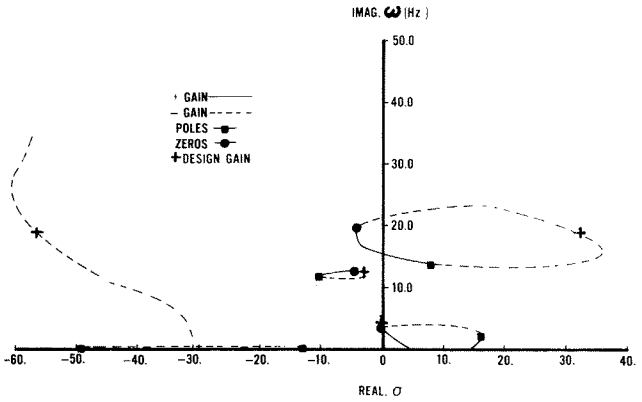

Figure 13 h Versus δ_{LE} Gain, Model Free in Pitch, V = 1.2 $V_{f_{p_2}}$

To control bending/torsion flutter, the trailing edge surface with angular acceleration feedback was again used. Figure 14 provides a root locus of the trailing edge loop with the leading edge loop closed (K_{LE} = -122 deg/in). This figure indicates that negative feedback stabilizes the 1st torsion mode; however it destabilizes the pitch mode over a large range of gains. Figure 15 shows gain loci with a phase lag network included in the trailing edge system compensation. For a τ of .1531, the instability in the pitch mode was eliminated. The feedback gain on the trailing edge loop was determined to be .026 deg/deg/sec^2. The design gains for each loop are marked on the loci in Figure 13 (leading edge loop) and Figure 15 (trailing edge loop).

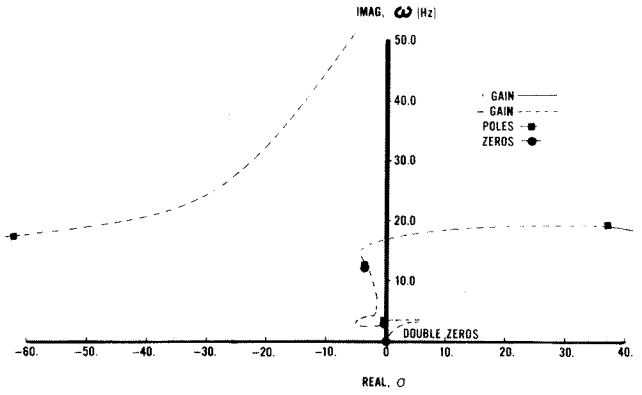

Figure 14 $\ddot{\alpha}$ Versus δ_{TE} Gain with K_{LE} = -122.0, Model Free in Pitch, V = 1.2 $V_{f_{p_2}}$

Figures 16 through 18 present the design data used in determining the two-surface control system gains when the model is free in both pitch and plunge. The poles shown in Figure 16 represent the rigid pitch mode and the three elastic modes. The plunge mode lies on the real axis. For this configuration, the two unstable modes have frequencies of 2.1 Hz and 13.9 Hz at 1.2 V_{fp2}. The rigid pitch mode and the 2nd bending mode are both stable at this airspeed and have frequencies of 1.6 Hz and 12.3 Hz,

respectively.

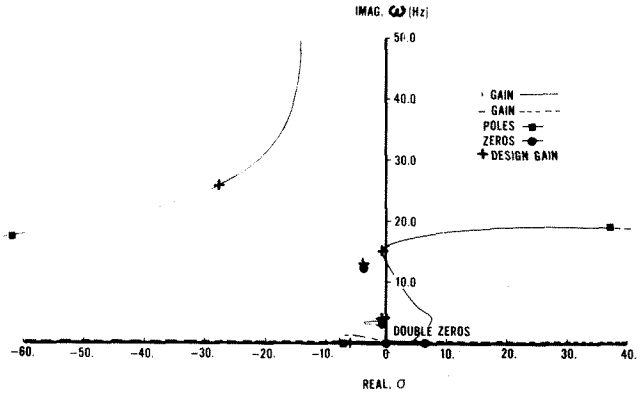

Figure 15 $\ddot{\alpha}$ Versus δ_{TE} Gain with K_{LE} = -122.0 and $\phi_{TE} = \frac{1 - .1531S}{1 + .1531S}$, Model Free in Pitch, V = 1.2 $V_{f_{p_2}}$

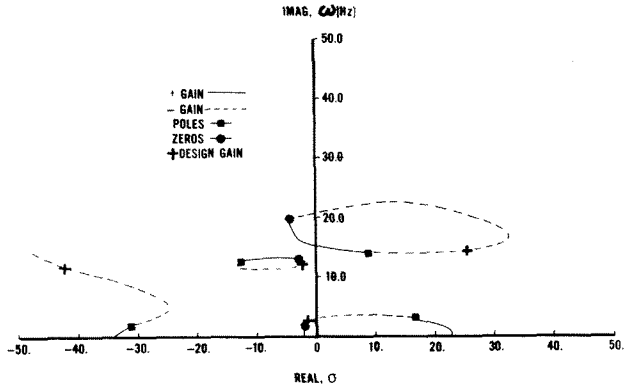

Figure 16 h Versus δ_{LE} Gain, Model Free in Pitch and Plunge, V = 1.2 $V_{f_{p_2}}$

Similar conclusions can be drawn regarding displacement feedback, as for the case when the model was free in only pitch. Calculations have shown that a system using h/δ_{LE} with negative feedback suppresses both modes of instability simultaneously at the design airspeed. However, analyses at off-design conditions again indicate that no system using only one surface could prevent both instabilities simultaneously over the entire velocity range of interest. Therefore, the two-surface approach defined previously was used to control the model free in pitch and plunge. A gain of -25.2 deg/in on the leading edge control surface with displacement feedback was required to improve the body freedom flutter instability up to the design airspeed with acceptable gain margins.

To determine a system for preventing the bending/torsion flutter mode, the leading edge system was closed and gain loci for the trailing edge system was determined (Figure 17). It was found that a trailing edge system gain of -.0203 deg/deg/sec^2 was necssary to obtain the required speed improvement and gain margins on the torsion mode. To obtain the best phase margins for this type of design, a phase lag network with a τ of .2144 was used (Figure 18).

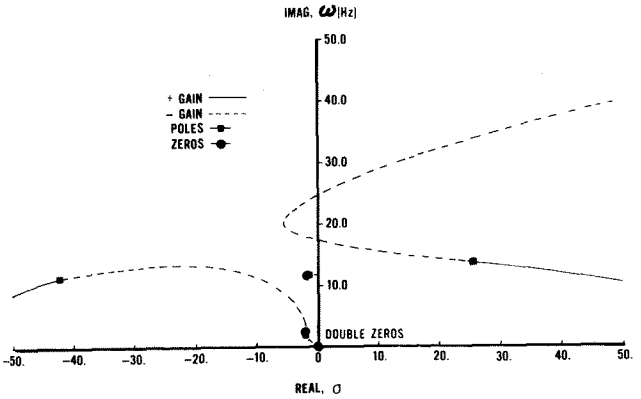

Figure 17 $\ddot{\alpha}$ Versus δ_{TE} Gain with K_{LE} = -25.2, Model Free in Pitch and Plunge, V = 1.2 $V_{f_{p_2}}$

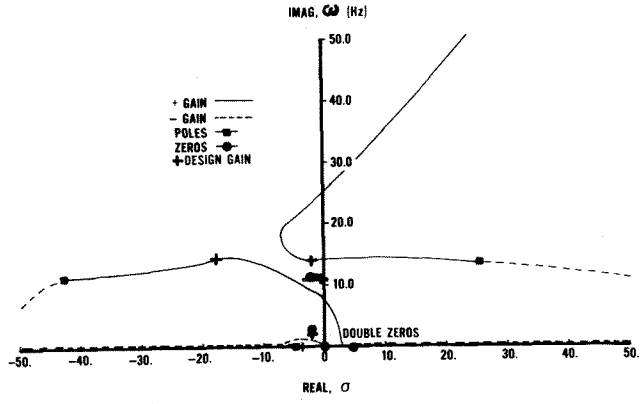

Figure 18 $\ddot{\alpha}$ Versus δ_{TE} Gain with K_{LE} = 25.2 and $\phi_{TE} = \frac{1 - .2144S}{1 + .2144S}$, Model Free in Pitch and Plunge, V = 1.2 $V_{f_{p_2}}$

The results of these studies indicated that a leading edge surface commanded by displacement of the wing resulting from only the elastic modes provided a reasonable control system design for preventing divergence of the cantilever wing or the body freedom flutter instability associated with the free model. Displacement at the wing sensor resulting from rigid model pitch and plunge were subtracted from the feedback signal to obtain only a response due to the elastic modes. The displacement sensor was positioned near the intersection of the wing 2nd bending node line and the wing 1st torsion node line. This location provided the best position for feeding back the bending motion of the 1st elastic mode (critical mode for divergence or body freedom flutter) with minimum inputs from the other important elastic modes.

The gain loci analyses also indicated that a trailing edge system commanded by angular acceleration of the wing tip perpendicular to the elastic axis provided an acceptable input for controlling the bending/torsion flutter mode. Based on mode shape data, the bending modes relative to the elastic axis had very little twist. Feeding back wing tip angular acceleration assured maximum input from the torsion mode (maximum twist at the tip) with minimum response from the bending modes.

The sensors used for measuring rigid pitch (angle of attack) and plunge (vertical translation) are located at the model center of gravity on the fuselage bar (pitch axis). For the analyses performed, the best overall suppression capability consisted of the leading edge and trailng edge control surfaces positioned in the same streamwise location on the wing at about 75 percent span. The schematic shown in Figure 19 illustrates the logic of the feedback system. It is important now to determine the performance of the control system over the entire velocity range of interest and to compare these data with the unaugmented results (Figures 7 through 9).

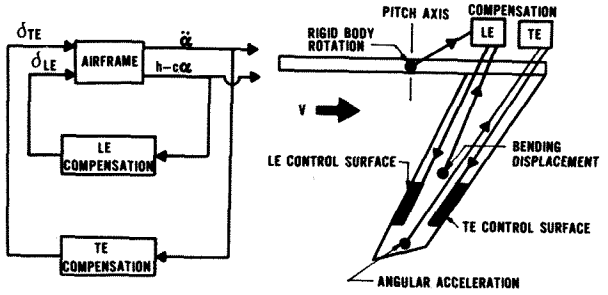

Figure 19 Schematic of Feedback System for Controlling Static Divergence and Flutter

V. Results

The velocity root locus for the cantilever wing two-surface control law is presented in Figure 20. This control system is shown to improve the velocity flight envelope of the cantilever model 63 percent based on the design criteria. With the system operating, flutter occurred in the 2nd bending mode at a speed of 188 ft/sec instead of in the torsion mode as was the case when the system was off. For the two-surface control law the gain margins at V_{fp} were calculated to be -6.19 db and 18.74 db on the leading edge loop, and minus infinity and 12.04 db on the trialing edge. The phase margins associated with the trailing edge loop were calculated to be -70 degrees and 25 degrees.

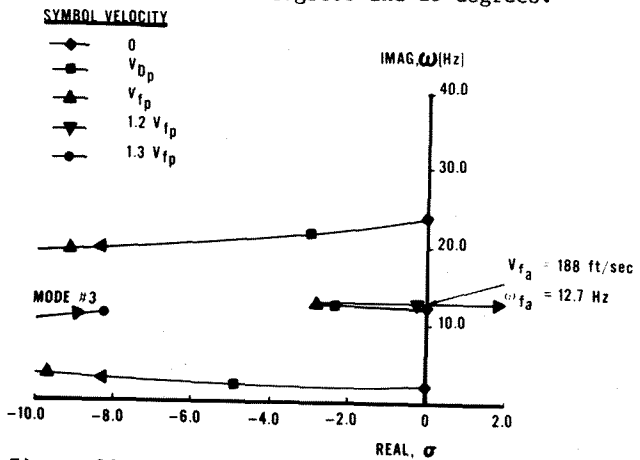

Figure 20 Root Locus for the Cantilever Wing, Nominal Two-Surface Control System (K_{LE} = -5.2, K_{TE} = .025, ϕ_{TE} = 155° @ 17 Hz)

The velocity root locus for the augmented model free in pitch is presented in Figure 21. This system was found to decouple the 1st bending and rigid pitch modes, and the 1st torsion and 2nd bending modes through the addition of aerodynamic stiffness. The increasing aerodynamic stiffness did, however, cause the 1st bending mode to become unstable at the design airspeed thus becoming the critical mode of interest. As a result of eliminating the body freedom flutter instability, the velocity flight envelope of the model free in pitch was increased 252 percent using the active system. The gain margins on the leading edge system were calculated to be -6.00 db and positive infinity, while the gain margins on the trailing edge system were found to be -12.74 db and 11.96 db. The phase margins were determined to be -13 degrees and 17 degrees on the trailng edge system.

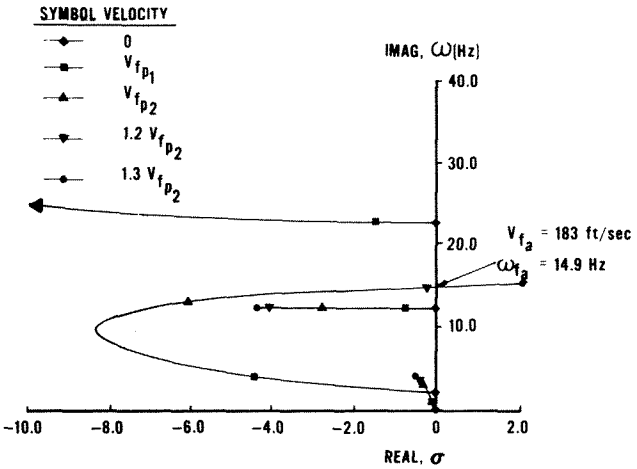

Figure 21 Root Locus for the Model Free in Pitch, Nominal Two-Surface Control System (K_{LE} = -122.0, K_{TE} = .026, ϕ_{TE} = 173° @ 17 Hz)

Figure 22 presents the closed loop results for the model free in pitch and plunge over the velocity range of interest. This control law performed well up to 1.2 V_{fp2} (182 ft/sec). At this speed two simultaneous instabilities were predicted to occur. The higher frequency instability was the bending/torsion flutter mode; the second instability was similar to the control induced instability that occurred in the 1st bending mode when the model was free in pitch only. For this case, however, the control induced instability was found to be a hump mode and was sensitive to changes in the feedback parameters. The flight velocity envelope expansion for this configuration was predicted to be 153 percent. The gain margins on the leading edge system at V_{fp2} were found to be -6.00 db and 9.36 db, and on the trailing edge system, -10.59 db and 6.19 db. The phase margins on the trailing edge system were calculated to be -59 degrees and 10 degrees.

Additional analyses were also performed to determine the sensitivity of the control law to changes in the feedback gain of each loop or to changes in the phase lag network. The next three figures present, in the form of stability

boundaries, the effects of changing one of the feedback parameters while holding the other two constant at nominal values. Only the results of the model free in pitch and plunge are presented. The stability boundary plots shown in Figures 23 through 25 were determined with respect to each of the feedback parameters K_{LE}, K_{TE}, and $_{LE}$. The solid circles on the boundaries represent data taken from the previous root locus plots, and the frequencies of the instability are shown in parentheses. The vertical dashed line represents the nominal control law. Gain and phase margins are easily determined from these figures. These margins are factors of safety that are established for a control system design. They are needed to account for the uncertainties, either neglected or unknown, that are encountered in an analysis.

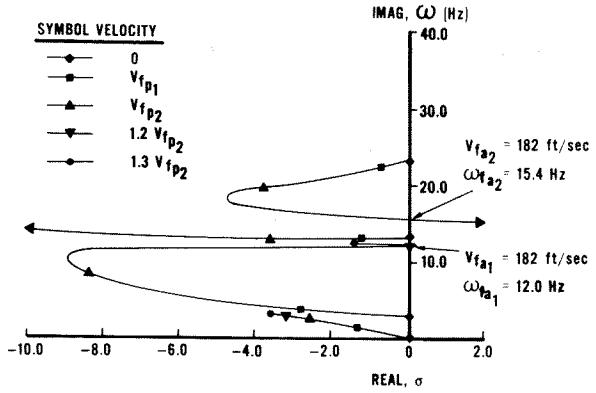

Figure 22 Root Locus for the Model Free in Pitch and Plunge, Nominal Two-Surface Control System (K_{LE} = -25.2, K_{TE} = .0203, ϕ_{TE} = 175° @ 17 Hz)

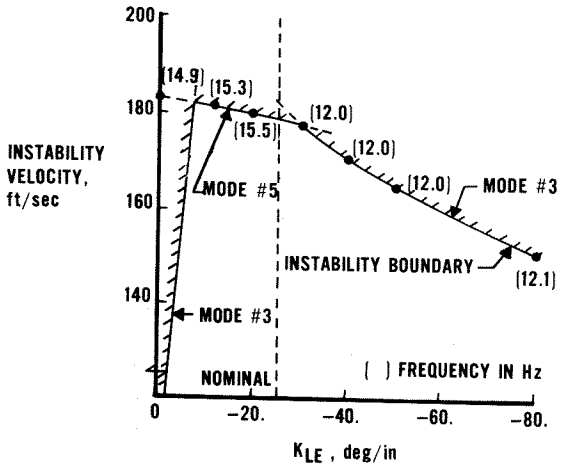

Figure 23 Stability Boundary with Variable K_{LE}, Model Free in Pitch and Plunge

VI. Conclusions

The studies reported herein have established the feasibility of applying active feedback control systems for preventing the aeroelastic instabilities associated with forward swept wings. The appliction of the concept for aeroelastic control is an efficient, adaptable, low weight approach compared to the classical

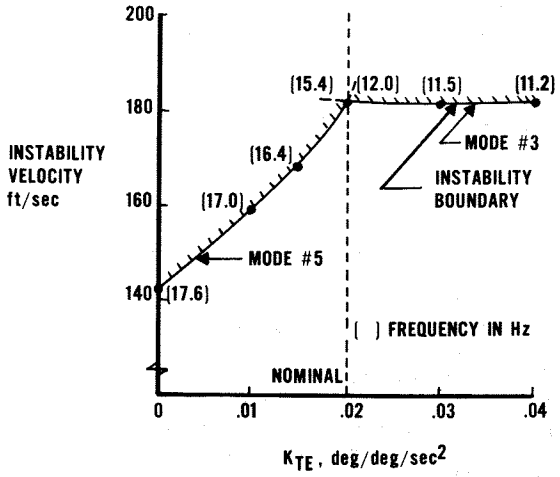

Figure 24 Stability Boundary with Variable K_{TE}, Model Free in Pitch and Plunge

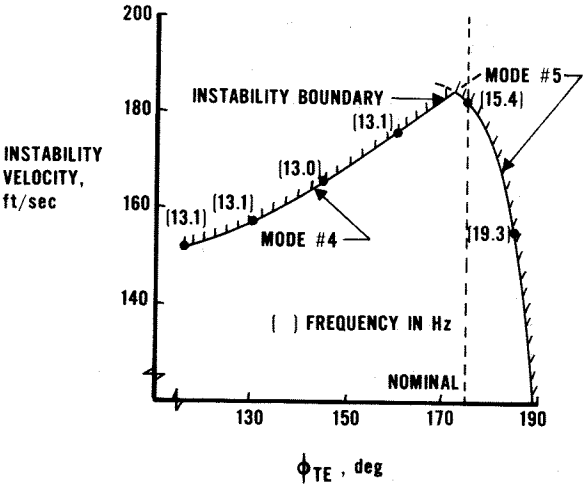

Figure 25 Stability Boundary with Variable ϕ_{TE}, Model Free in Pitch and Plunge

techniques of adding weight, stiffening the wings, or imposing aircraft speed placards. The classical approaches for flutter and divergence prevention have historically resulted in a loss of aircraft performance. With the advent of high-gain digital/adaptive flight control systems, it is easily conceivable that the flutter and divergence control systems could become integral parts of the flight control system using common components designed for reliability and redundancy.

It is speculated that an active system for aeroelastic control would be most beneficial when one considers damaged composite wings resulting in a loss of stiffness, or the external store carriage issue that causes many flutter problems. An adaptive control system, a logical extension of the concept studied, offers significant promise for the external store flutter issue.

It is expected that an active control system will be initially used to obtain speed margins of safety (15 percent above the aircraft maximum speed). The system in this case would be operating at speeds near the aircraft maximum

speed but the vehicle would never be operating at a passively unstable flight condition. As more confidence is developed for such a system, it would probably be used to prevent aeroelastic problems that are occuring deep within the flight envelope of the vehicle (external store flutter problem). Large payoffs in terms of aircraft performance are expected as a result of this application.

As a result of these and other active flutter suppression and divergence analyses on cantilever wings and wings with rigid modes, the tools for designing linear systems appear to be available. However, there are several important analytical and experimental aspects related to this subject that require additional investigation. From an analytical viewpoint, the effects of Mach number and dynamic pressure should be evaluated to form sensitivity trends. Furthermore, variables such as static margin and forward sweep angle should be addressed. These sensitivity trends may define the need for adaptive control laws for variable flight conditions in addition to the need of such a system for external store applications. Regarding aerodynamics, the effects of nonlinearities in the transonic flow region need to be evaluated. Also, alternate design procedures involving the time domain need to be further developed to evaluate these and other nonlinearties.

There is currently a need to demonstrate through wind tunnel tests, the suppression of divergence on a cantilever wing using displacement feedback. Evaluations of the effects of symmetric rigid body modes such as rigid pitch and plunge on the suppression of body freedom flutter should also be seriously considered using wind tunnel models.

Analyses and wind tunnel tests also need to be conducted to evaluate the antisymmetric rigid and elastic modes of a forward swept wing to determine if other unexpected aeroelastic instabilities are not hidden in the shadows of simplifying assumptions. Finally, free-flying wind tunnel models incorporating all six rigid body degrees of freedom need to be used to investigate the feasibility and practicality of active aeroelastic control systems.

References

1. Krone, N., "Divergence Elimination with Advanced Composites", AIAA Aircraft Systems and Technology Meeting, Los Angeles, California, Aug 1975.

2. Griffin, K. E., and Eastep, F. E., "Active Control of Forward Swept Wings with Divergence and Flutter Aeroelastic Instabilities", AIAA Paper No. 81-0637, Atlanta, GA, Apr 1981.

3. Weisshaar, T. A., "Divergence Suppression of Forward Swept Wings", Final Report NASA Grant, NASI-15080-Task 16, Virginia Polytechnic Institute and State University, Sep 1980.

4. Weisshaar, T. A., Zeiler, T. A., Hertz, T. J., and Shirk, M. H., "Flutter of Forward Swept Wings, Analysis and Test", paper presented at the 23rd AIAA SDM Conference, New Orleans, LA, Apr 1982.

5. Gaukroger, D. P., "Wind Tunnel Flutter Tests on Model Delta Wing under Fixed and Free-Root Conditions", British A. R. C., R&M 2826, 1955.

6. Cunningham, H. J., and Lundstrom, R. R., "Description and Analysis of a Rocket-Vehicle Experiment on Flutter Involving Wing Deformation and Body Motions", NACA TN-3311, Jan 1955.

7. Miller, G. D., Wykes, J. H., and Brosnan, M. J., "Rigid Body-Structural Mode Coupling on a Forward Swept Wing Aircraft", Paper No. 82-0683, New Orleans, LA, May 1982.

8. Chipman, R. R., Zislin, A. M., and Waters, C., "Active Control of Aeroelastic Divergence", Paper No. 82-0684, New Orleans, LA, May 1982.

9. Noll, T. E., Eastep, F. E., and Calico, R. A., "Active Suppression of Aeroelastic Instabilities on a Forward Swept Wing" Paper presented at the 24th AIAA SDM Conference, Lake Tahoe NV, May 1983.

10. Noll, T. E., Calico, R. A., and Eastep, F. E., "Control of Forward Swept Wing Aeroelastic Instabilities Using Active Feedback Systems", paper presented at the AIAA Guidance and Control Conference, Gatlinburg, TN, Aug 1983.

11. Giesing, J. P., Kalman, T. P., and Rodden, W. P., "Subsonic Unsteady Aerodynamics for General Configurations", AFFDL-TR-75-5 Part I, Vols I and II, Nov 1971.

12. Baker, G. A., "Essentials of Pade Approximates", Academic Press, 1975.

13. Vepa, R., "On the Use of Pade Approximates to Represent Unsteady Aerodynamic Loads for Arbitrary Small Motions of Wings", AIAA Paper No. 76-17, Jan 1976.

14. The NASTRAN User's Manual, (Level 17.0), NASA SP-222 (04), National Aeronautics and Space Administration, Dec 1979.